City Research Online

City, University of London Institutional Repository

This is the accepted version of the paper.

This version of the publication may differ from the final published version.

Permanent repository link: http://openaccess.city.ac.uk/21562/

Link to published version: http://dx.doi.org/10.4271/2019-01-0066

City Research Online: http://openaccess.city.ac.uk/   publications@city.ac.uk

Simulation and measurement of Transient Fluid Phenomena within Diesel Injection

Author, co-author (Do NOT enter this information. It will be pulled from participant tab in MyTechZone)

Affiliation (Do NOT enter this information. It will be pulled from participant tab in MyTechZone)

Abstract

Rail pressures of modern diesel fuel injection systems have increased significantly over recent years, greatly improving atomisation of the main fuel injection event and air utilisation of the combustion process. Continued improvement in controlling the process of introducing fuel into the cylinder has led to focussing on fluid phenomena related to transient response. High-speed microscopy has been employed to visualise the detailed fluid dynamics around the near nozzle region of an automotive diesel fuel injector, during the opening, closing and post injection events. Complementary computational fluid dynamic (CFD) simulations have been undertaken to elucidate the interaction of the liquid and gas phases during these highly transient events, including an assessment of close-coupled injections.

Microscopic imaging shows the development of a plug flow in the initial stages of injection, with rapid transition into a primary breakup regime, transitioning to a finely atomised spray and subsequent vaporisation of the fuel. During closuring of the injector the spray collapses, with evidence of swirling breakup structures together with unstable ligaments of fuel breaking into large slow-moving droplets. This leads to sub-optimal combustion in the developing flame fronts established by the earlier, more fully-developed spray. The simulation results predict these observed phenomena, including injector surface wetting as a result of large slow-moving droplets and post-injection discharge of liquid fuel. This work suggests that post-injection discharges of fuel play a part in the mechanism of the initial formation, and subsequent accumulation of deposits on the exterior surface of the injector. For multiple injections, opening events are influenced by the dynamics of the previous injection closure; these phenomena have been investigated within the simulations.

Introduction

Fuel injector technology and injection strategies used in diesel and gasoline engines have developed significantly over recent years. All new passenger car diesel engines, and a significant proportion passenger car gasoline engines, sold in the EU now have direct-injection (DI) combustion systems. To assist in enhanced control of combustion for improved fuel consumption and hence reduced CO_2 and other emissions, maximum rail pressures of both diesel and gasoline engines are constantly increasing. Peak values for emerging diesel fuel injection systems are ≥ 2500 bar (250 MPa) [2-4] and those for DI gasoline engines 350 bar [5,6], with values up to 500 bar on the horizon [7]. The ratio of diesel injector pressure capability to that of gasoline injectors is now less than one order of magnitude, compared with well over two orders of magnitude when only port-fuel-injected gasoline engines were available in the market.

Combustion strategies for both diesel and gasoline engines rely on multiple injections of fuel to improve combustion efficiency and reduce pollutant emissions, either the level emanating directly from the cylinder or to help activate catalysts to control the level which are released from the exhaust tail-pipe. Multiple fuel injection strategies are also used to reduce combustion noise. Whilst increasing injection pressure offers benefits in terms of fuel atomisation and combustion phasing at higher engine loads and speeds, it can increase the challenge of controlling the spray quality at the lower fuel rail pressure required to reduce fuel pump work at lower load operation. The control of fuel delivery is especially important in the "off design" parts of the injection event, namely at the start and end of the process. The present work focusses on these transient parts of the injection event in diesel engines.

The challenge of controlling individual injection events is intensified by the use of multiple injections with short separations between each event. Multiple injection strategies, such as digital rate shaping (DRS) [4,8], allow the use of a variety of options for pilot, main, and post-(main) injection events in order to provide a degree of control over the timing and phasing of the ignition delay and heat release events. Using this approach it is possible to reduce combustion noise whilst remaining within acceptable particle emissions levels. Figure1 shows DRS injection sequences that may be employed to meet the emissions and noise control demands of modern diesel engines. The sequence of initial injections controls the pre-mixed fuel quantity and subsequent energy release ahead of the main and post-injection event. The development of features such as needle closing sensors (NCS) are an indication of the importance of controlling the fuel metering to the engine through the life of the fuel injector [4].

The use of the complex strategies described above relies on the ability of the fuel injection equipment to accurately meter extremely small quantities of fuel per event (which may be of the order of 1 mg of fuel being injected in a period of less than 0.5 ms) over the engine lifetime. During these short metering events the injector will not reach full lift and will be operating within the transient part of the rate curve. These demands, together with the use of nozzle holes with diameters in the region of 100 µm [9] mean that it is extremely important to avoid the accumulation of excessive carbonaceous deposits on, and within the fuel injector, such as those shown in Figure 2.

Deposits can accumulate on the interior or exterior of a fuel injector (in gasoline and diesel engines). Internal deposits (within the injector

7/20/2015

body itself) can lead to sticking needles which can affect engine drivability and emissions. Nozzle hole deposits can reduce the effective flow area of the fuel (a 10μm deposit layer within a 100μm injector nozzle hole reduces the geometric area by over 35%) [11] or cause it to be mis-directed. These effects give rise to poorer atomisation and mixing, excessive spray penetration, and increased risk of fuel impacting on the combustion chamber surfaces, with the potential to adversely affect emissions. The accumulation of deposits on the injector tip can absorb fuel.
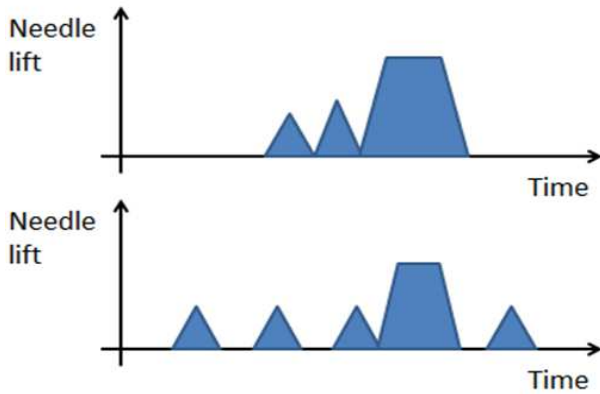

Figure 1. Generic options for fuel injection strategy used in modern diesel engines at part-load to meet emissions and noise requirements.

Investigations using high speed photography have been carried out for several decades [10,11]. The impact of the deposits within nozzle holes and their effect on engine performance are now better understood [11] but the physical and chemical mechanisms which lead to initial attachment and growth of deposits in the holes or on the surface of the injector are still being investigated though out the automotive industry. The ingress of gas at the end of injection has been identified by some authors [30, 34] while Kalghatgi [11] summaries the literature well concluding that residual fuel remaining within the injector nozzle is thought to be instrumental in the process [9].

The present paper focuses on the ability of diesel injectors to control the early and late phases of the fuel injection event. The paper includes some previously published and new images which, together, show how the highly dynamic evolution and collapse of the spay lead to very different fuel morphologies to those which prevail when the spray is fully developed. The previously published images are reviewed here from the perspective of their potential role in the formation of deposits on the exterior of diesel injectors, including those which form within nozzle holes. These data will compliment studies with both ECN and full geometry injector with simulation and experimental comparison for diesel injection events. [18-33]

The images shown of the end of the injection event indicate that it is likely that the large ligaments of liquid fuel which emerge in this period with poor combustion characteristics [36] or lead to wetting of the surface of the fuel injector. Images are also included which show the discharge of fuel from the nozzle after the injection event wetting the surface of the fuel injector. In addition images reveal combustion occurring in the vicinity of the wet surface of clean fuel injectors are shown – it is possible that these phenomena are important in the initial generation of carbonaceous deposits and subsequent accumulation.
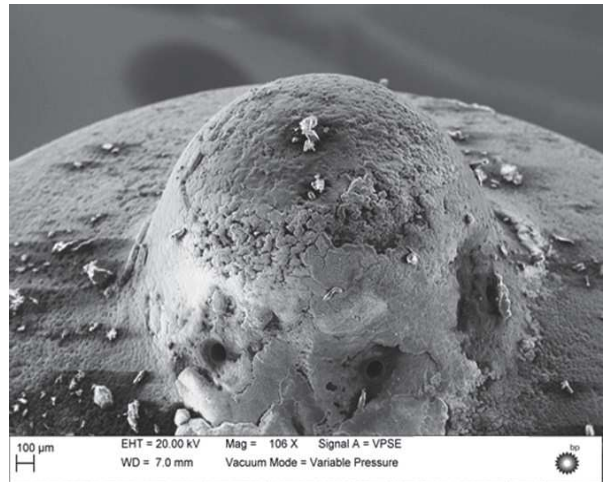
Figure 2. Deposits on the external surface of a diesel fuel injector.

Analysis Techniques

Rig, Operating Conditions and Optical Approach

The majority of the images of fuel injector sprays and transient fluid flow phenomena were produced in the reciprocating rapid compression machine (RCM) facility at the University of Brighton. The RCM is a single-cylinder, two-stroke engine with a bore of 135mm and a stroke of 150 mm, giving a displacement of 2.2 litres. This relatively large cylinder volume enables good optical access to capture events under high pressure and temperature ambient conditions. The fuel injection equipment consists of a number of classical common rail components, with the high pressure fuel pump being electrically driven and connected to a common rail system capable of delivering a rail pressure of up to 2000 bar (200 MPa). The present data set focuses on a diesel injector of VCO (valve covers orifice) design. A detailed description of the test rigs are covered by Crua [14, 15]. For increased clarity of imaging, several start of injection data sets were captured under atmospheric conditions.

Operating conditions in the RCM were chosen to represent a range of engine operating conditions from idle to medium load. In-cylinder pressures (ICPs) were 40 to 100 bar (4 to 10 MPa) and fuel injection pressures were between 400, 1000 bar (40 – 100 MPa). Estimated in-cylinder temperature was in the range of 700-760 K at the point of fuel injection, using. EN 590 diesel fuel. For the work focussing on the end of the injection event, the fuel was injected for 500 μs (TTL trigger duration) with the event beginning at 3° before top dead centre (BTDC). High speed animations were captured at different times after the start of injection (0.3-1.5 ms).

Figure 3 shows the optical set up used to generate the images at the end of the injection event. It can be seen that a dual illumination approach is used with two lasers acting as light sources. The camera used was a Phantom v12.1 12 bit high-speed CCD unit recording at 160 x152 pixels resolution for a total of 85 frames which allowed a maximum frame rate of 10 kfs. The scale factor was 3.48 μm / pixel to give a field of view of 529 μm x 557μm. Illumination was first achieved using a CAVILUX Cavitar 690 nm solid state diode laser. For later experiments the dual-illumination setup was used with an external trigger being provided by a pulse generator.
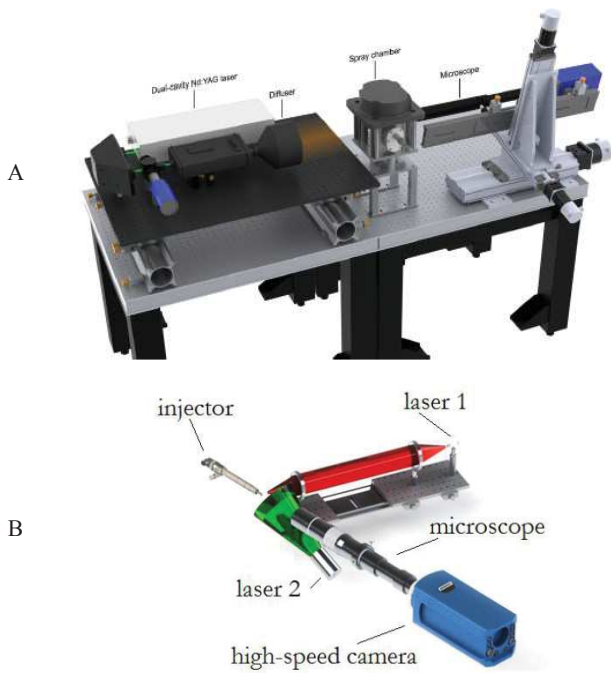
Figure 3. Optical arrangements used to study fuel injection dynamics around the injector tip. A) Detailed imaging setup, atmospheric rig which was transferred to the RCM, B) High speed imaging arrangement

Computational Fluid Dynamics (CFD)

Full 360° geometry simulations are performed of diesel injection using a RANS (Reynolds Averaged Navier-Stokes) approach, built within a customized setup of ANSYS Fluent. The simulations capture the fuel flow within the nozzle and its exit into the surrounding gas domain, for a similar VCO injector to the measurements (Delphi DFI 1.3, 7 hole VCO, 135μm nozzle exit with 154° cone angle). The simulation injector has 6 holes with size of 161μm at the orifice entrance and 128μm at the orifice exit (k-factor 3.3), with a nozzle hole length of 1mm.

The computational methodology is based on a sharp interface 'volume of fluid' (VOF) technique including several customized models, which can track the liquid/non-condensable gas interface [19]. A three-phase fully compressible barotropic cavitation model is employed [19], where pressure is related to density, capturing phase change at saturation pressure, combined with non-condensable gases. K-omega turbulence modelling with corrections in presence of cavitation was implemented, is discussed in [23], the original model is from Reboud et al. [21]. Standard two layer wall functions were used, including turbulence corrections in the presence of the immersed boundary, based on [22].

The computational mesh (Figure 4) is purely hexahedral, to maintain a good quality and minimise numerical diffusion. It is split in two domains: one involving the injector interior up to the orifice exit and the other comprising a spatial region external to the injector, into which the fluid travels. Non-conformal mesh refinement is applied in order to capture details of atomization at the orifice exit. The total mesh contains ~6 million cells inside and ~4 million cells in the injector exterior region. Key areas of interest were the nozzle exit flow and assessment of liquid impingement on the injector surface. The mesh distribution allows for good resolution within these

boundary layers and the needle. In particular, near wall resolution around the needle seat is 0.5μm, with 1.75μm near the orifice walls. Resolution in the orifice core is 5μm. To maintain an affordable simulation the mesh was coarsened downstream of the nozzle, with larger cell aspect ratios which could influence some droplet shaping.

The inlet boundary at the top of the simulation domain, is initialised with high pressure liquid fuel (no vapour, no air) at 1600 bar and 60°C, which is typical of the thermal conditions within the high pressure fuel rail. The orifice exit is initialized as non-condensable gas (ambient air) at a downstream pressure of 60bar. The domain from needle/seat contact to the orifice exit is initialised at the same downstream pressure and is full with liquid fuel.

The needle moves in a full three-dimensional space. Thus, apart from the axial component of motion (z-direction), there is an eccentric motion component in the x and y directions (see figure 5). The data presented was gathered from the x-ray measurement of a needle motion within an operating injector. This accurate representation of the asymmetry within the simulation will offer realistic variation in flow phenomena between each hole around the nozzle.
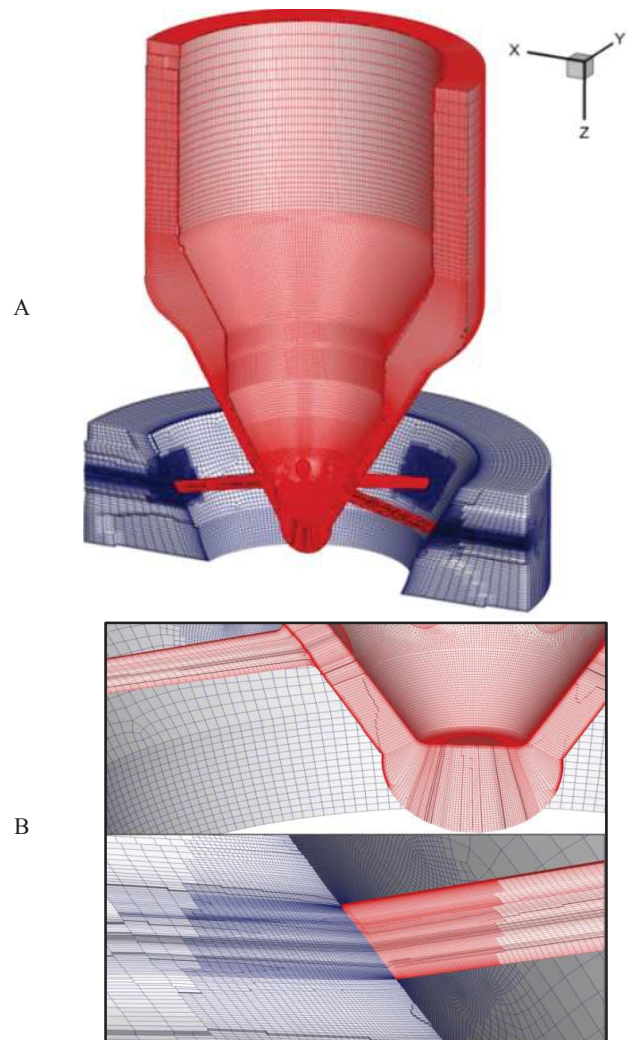

Figure 4:. A)Computational mesh: (A)rRed mesh corresponds to the domain inside the injector; blue mesh corresponds to the exterior. B) Details of mesh refinement in the orifice and at the orifice exit.
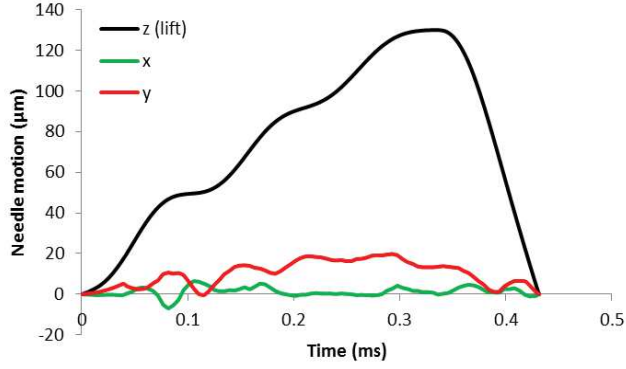
Figure 5. Needle movement profile, including eccentric motion.

Numerical Model

The numerical formulation used for modelling three-phase cavitation and the immersed boundary is explained below including key governing equations.

Three-Phase Model

The cavitation model used in this study is based on homogeneous equilibrium assumption which uses a barotropic equation of state for modelling the pressure density relationship of each phase. The barotropic relationship employed here is a piece-wise function as given in Eq.(1).

$$p = \begin{cases} B\left[\left(\frac{\rho}{\rho_l}\right)^N - 1\right] + p_{sat,l} & \rho \geq \rho_l \\ \frac{c_v^2 c_l^2 \rho_l \rho_v (\rho_v - \rho_l)}{c_v^2 \rho_v^2 - c_l^2 \rho_l^2} \ln\left(\frac{\rho}{c_l^2 \rho_l (\rho_l - \rho) + c_v^2 \rho_v (\rho - \rho_v)}\right) + p_{ref} & \rho_v \leq \rho \leq \rho_l \\ C_{vap}\rho^\kappa & \rho < \rho_v \end{cases} \quad (1)$$

where, B and N are the bulk modulus and stiffness of liquid, subscripts l and v refers to pure liquid and vapour phases, c is the speed of sound, ρ is the density. $p_{sat,l}$ and p_{ref} are tuned to have a continuous variation of pressure and density between the liquid and mixture phase. C_{vap} and κ are the isentropic constant and heat capacity ratio of pure vapour.

The equation is fully compressible, with the use of Tait equation for modelling liquid compressibility, isentropic gas for pure vapour phase and the pressure density relationship for the mixture phase is derived by integrating Eq.(2) for an isentropic process with the speed of sound defined using the Wallis formulation. A detailed derivation of this model can be found in [23]. The values of the parameters in Eq.(1) are listed in Table 1.

$$c_{wallis}^2 = \left(\frac{\partial p}{\partial \rho}\right)_s \quad (2)$$

The third phase, the non-condensable gas (air) is modelled as an additional phase with no mass transfer between the liquid/vapour phase using the mixture approach. The barotropic relationship for the non-condensable gas is based on the isentropic gas equation as given in Eq.(3).

$$p = C_{gas}\rho^\gamma \quad (3)$$

where, C_{gas} is the isentropic gas constant and γ is the heat capacity ratio for air. The three-phase mixture density and the volume fraction of the vapour phase is calculated using Eq.(4) and Eq.(5) respectively.

$$\rho_m = (1 - \alpha_g)\rho_{lv} + \alpha_g\rho_g \quad (4)$$

$$\alpha_v = (\rho_l - \rho_{lv})/(\rho_l - \rho_v) \quad (5)$$

where, the subscripts m, lv and g refers to the three-phase mixture, barotropic fluid and non-condensable gas phases respectively and α is the volume fraction.

Liquid Properties			Vapour properties			Gas Properties		
B	193	MPa	C_{vap}	17036.5	pa/ (kg/m³)ⁿ	C_{gas}	75267.8	pa/ (kg/m³)$^\gamma$
N	7.15	--	κ	1.023	--	γ	1.4	--
$\rho_{sat,L}$	880.71	Kg/m³	$\rho_{sat,V}$	0.143	Kg/m³			
$C_{sat,L}$	1253	m/s	$C_{sat,V}$	129.1	m/s			
$P_{sat,L}$	54885.6	Pa	$P_{sat,V}$	2336.2	Pa			
μ_L	4.63e-03	Pa s	μ_V	7e-06	Pa s	μ_g	1.78e-5	Pa s

Table 1: Thermodynamic properties for diesel liquid/vapour and ambient gas
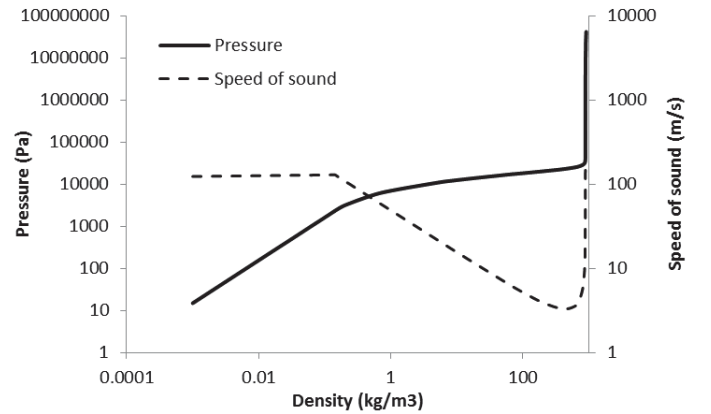

Figure 6: Diagram showing the variation of pressure and speed of sound in relation to density for diesel liquid/vapour

Governing Equations

The three-phase flow is governed by the continuity and momentum equation describing the motion of the mixture. The averaged form of the governing equation employed for the RANS (Reynolds Averaged Navier-Stokes) simulations are:

$$\frac{\partial}{\partial t}(\rho_m) + \frac{\partial}{\partial x_j}(\rho_m u_j) = 0 \quad (6)$$

Page 4 of 19

7/20/2015

$$\frac{\partial}{\partial t}(\rho_m u_i) + \frac{\partial}{\partial x_j}(\rho_m u_i u_j) = -\frac{\partial p}{\partial x_i} + \frac{\partial}{\partial x_j}(\tau_{ij}) + \frac{\partial}{\partial x_j}\left(-\rho_m \overline{u_i' u_j'}\right) + f_{IB} \tag{7}$$

where ρ_m is the mixture density, u is the velocity vector, p is the pressure, $-\rho_m \overline{u_i' u_j'}$ are stresses arising from Reynolds averaging and τ_{ij} is the stress tensor defined as:

$$\tau_{ij} = \frac{\partial}{\partial x_j}\left(\mu\left(\frac{\partial u_i}{\partial x_j} + \frac{\partial u_j}{\partial x_i}\right) - \frac{2}{3}\delta_{ij}\left(\frac{\partial u_l}{\partial x_l}\right)\right) \tag{8}$$

In Eq.(8), μ is the viscosity of the mixture, and δ_{ij} is the Kronecker delta. The Reynolds stresses are modelled using the k-ω SST model, following the Boussinesq hypothesis:

$$-\rho_m \overline{u_i' u_j'} = \mu_t\left(\frac{\partial u_i}{\partial x_j} + \frac{\partial u_j}{\partial x_i}\right) - \frac{2}{3}\delta_{ij}\left(\rho_m k + \mu_t \frac{\partial u_l}{\partial x_l}\right) \tag{9}$$

For the closure of turbulence model, two additional equations are solved, one for turbulent kinetic energy, k, and the other for specific turbulent dissipation rate, ω, as follows:

$$\frac{\partial}{\partial t}(\rho_m k) + \frac{\partial}{\partial x_j}(\rho_m u_j k) = \frac{\partial}{\partial x_j}\left(\Gamma_k \frac{\partial k}{\partial x_j}\right) + G_k - Y_k + Su_k \tag{10}$$

$$\frac{\partial}{\partial t}(\rho_m \omega) + \frac{\partial}{\partial x_j}(\rho_m u_j \omega) = \frac{\partial}{\partial x_j}\left(\Gamma_\omega \frac{\partial \omega}{\partial x_j}\right) + G_\omega - Y_\omega + Su_\omega \tag{11}$$

where, Γ, G, Y and Su are the effective diffusivity, turbulent production, dissipation and user defined source terms. The definitions can be found in [22]. In addition to the correction implemented for eddy-viscosity in the SST model to avoid the over prediction of its value, an additional correction for the density term is implemented in the calculation of eddy-viscosity to compensate for the compressibility of the liquid-vapour mixture [21] as given below:

$$f(\rho) = \rho_v + (1-a)^{10}(\rho_l - \rho_v) \tag{12}$$

$$\mu_t = f(\rho)\frac{a_1 k}{\max(a_1 \omega, S F_2)} \tag{13}$$

where, a is the vapour volume fraction, the subscript l and v refers to liquid and vapour, a_1=5/9, S=$(2S_{ij}:S_{ij})^{0.5}$ with S_{ij} being the strain rate tensor and F_2 is the blending function. The source terms f_{IB}, Su_k and Su_ω are implemented to account for the immersed body and their implementation is explained in the next section. Air is tracked as an additional transport equation, represented with the index g, following the conservation formula:

$$\frac{\partial}{\partial t}(\rho_g a_g) + \frac{\partial}{\partial x_j}(\rho_g a_g u_j) = 0 \tag{14}$$

Immersed Boundary Model

In order to maintain interface sharpness, an implicit VOF technique is used. The technique is based on a high order interface capturing model, termed as CICSAM [37].

Due to the small clearances and the irregular motion between the needle and the needle seat, the canonical body fitted grids with remeshing/deforming approaches can be computationally expensive and inefficient. On the other hand, in an immersed boundary method (IBM), the presence of a body is represented using a forcing term in the momentum equation. The IBM approach used in this study is based on the *continuous forcing* approach [37], with methodology published in [20], and has allowed the initial conditions of the simulation to incorporate a fully closed needle geometry.

The forcing tem (f_{IB}) is added to the continuous form of momentum equation as shown in Eq.(7). It is the source term that forces the flow to follow the motion of the immersed body. This force is proportional to the difference in flow velocity ($\bar{u}$) and the target body velocity ($\bar{U}_{IB}$; which is the velocity of the immersed body). The formulation of the forcing term is given in Eq.(15).

$$f_{IB} = -\frac{\rho C}{dt}\alpha_{IB}(\bar{u} - \bar{U}_{IB}) \tag{15}$$

In the above equation, C is an arbitrary coefficient which can be tuned to adjust the strength of the immersed body velocity, dt is the time step and α_{IB} is the masking function which takes a value of 1 if the cell is inside the immersed body (solid) and 0 if the cell is outside (fluid). Any value between 0 and 1 refers to a cell which is partially occupied by the wall. For calculating the mask function in each cell, the wall normal distance of each cell nodes from the immersed boundary points is estimated and the IB point with the minimum distance is identified. The formulation of this can be represented using Eq.(16) where $\bar{x}_n$ and $\bar{X}_{IB}$ are the coordinates of the cell node and immersed boundary point, n_{IB} is the normal to the wall. The distance from the immersed body to the cell is estimated as the average of node distances Eq.(17) After estimating the distance function from Eq.(16), the mask function α_{IB} in Eq.(15) is calculated using Eq.(18).

$$d_{n,IB} = (\bar{x}_n - \bar{X}_{IB}).n_{IB} \quad \text{if } min(|\bar{x}_n - \bar{X}_{IB}|) \tag{16}$$

$$d_{c,IB} = \frac{\sum_n d_{n,IB}}{n} \tag{17}$$

$$\alpha_{IB} = \frac{\sum_n d_{n,IB} < 0}{\sum_n |d_{n,IB}|} \tag{18}$$

When the immersed body is moved, the Eulerian cells inside the immersed body should have the same velocity as the body. The source terms in the turbulence equations are defined in a way that satisfies the conditions of k=0 and $\omega\rightarrow\infty$ (10^{15} 1/s for this study).

Spray Development and Collapse

As the number of injection events increases, the portion of injection time spent during the transient spray developing or collapsing phases increases, and hence a greater proportion of off-design injection spray. Fuel injection manufacturers are striving to develop fast opening and closing injection hardware constrained by the finite needle inertia and bulk modulus of the fuel. Below a defined duration of driving the injector action, the needle can be in ballistic mode (where its motion is uncontrolled by the solid mechanical stops) for the whole injection event and hence there would be no period in which the spray approximates to that of a fully-developed steady-state condition. During these 'transient' portions of the injection event the atomisation characteristics are significantly different to those which exist in the portion of the event where spray could be considered to be in a fully-developed condition.

Fully Developed Sprays

Many analyses of diesel injection events have been conducted at a macroscopic level, assessing spray penetration and divergence. Since these sprays are dense, fast moving events, application of other diagnostic tools has proved difficult. It has, however, been possible to apply microscope imaging techniques to investigate diesel injection, being previously demonstrated by the authors [13, 14].

Due to the high magnification required to understand the detailed phenomena within the nozzle hole exit region and adjacent surface, the field of view within one frame is 600 microns. This offers detailed analysis of droplets and ligaments but precludes the macroscopic view of the whole spray. In order to combine the microscopic detail with the macroscopic view of a fully developed injection event, a montage of microscopic images is presented in Figure 7, recorded 1ms after start of injection (ASOI). This image of a fully-developed spray is built up from a series of smaller images of different injection events detailing the atomization processes along the spray boundary. The spray core has been filled to simulate the dense spray which can not be assessed for detailed information.

It can be seen that, as the dense core of the spray penetrates the gas ahead, it diverges and fine droplets are created around the spray interface. This atomisation is a consequence of the liquid shearing with the surrounding gas, creating local eddy structures and entraining some of the gas into the spray boundary. The repeatability of the injection and atomization process is evident by the fact the first 60-70% of the microscopic images knit well together even though they are captured from separate injection events. Further down-stream, towards the leading edge of the injected spray, the shearing and gas entrainment results in a more well mixed zone. This is evident from lower levels of obscuration and variation in density gradients within the gas phase from droplet vapour and thermal gradients from evaporation. This area has higher variability due to the stochastic nature of the turbulent mixing process.

Two high resolution images from the leading edge region (Figure 8) demonstrate the details of entrainment and evaporation. Image A is located 20mm from the orifice, while image B is 24mm from the nozzle hole on spray axis.

Within image A the gradation from the dense core of the spray, to the fine liquid droplets at its extremities, are evident. These droplets have been sheared by the relative motion of the liquid and the surrounding gas, while the gas entrainment in to the spray is apparent. Image B

illustrates the leading edge droplets and spray structure. It reveals evidence of density trails behind droplets, a consequence of thermal gradients plus droplet evaporation. In addition, the intensity of shearing and associated turbulence and overall penetration velocities, results in the formation of droplets which are not necessarily spherical.
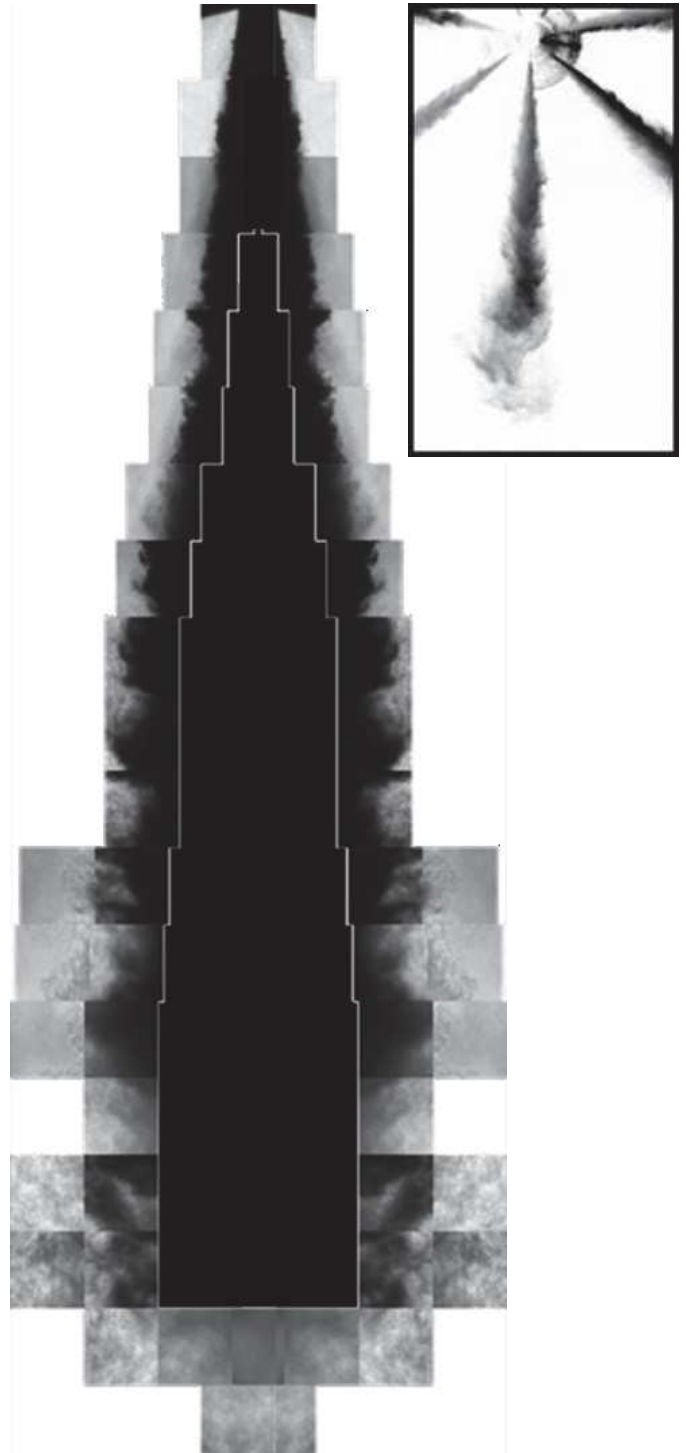

Figure 7. Montage of images from individual spray events to form a high-resolution representation the spray interface of a fully developed spray. [14]
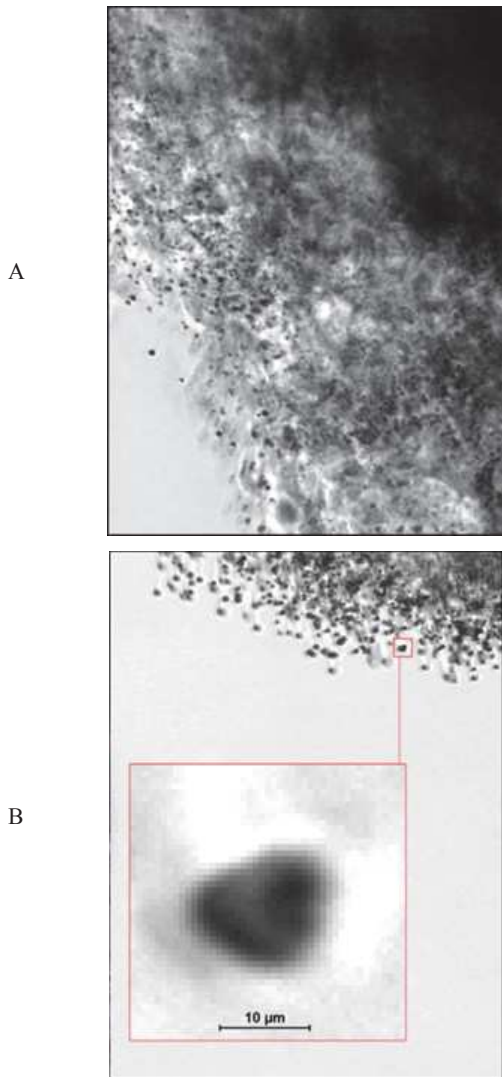
A

B

Figure 8. Higher magnification shadowgraphic image of the leading edge of the spray event shown in Figure 7. (Injection at 400 bar into gas at 32 bar pressure and 700 K bulk temperature) [13]
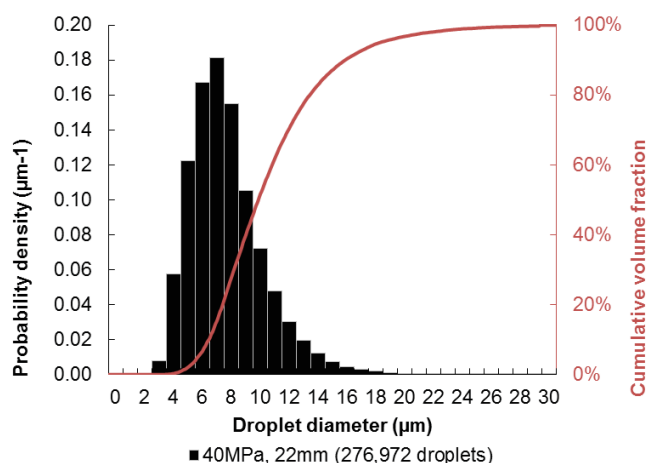

Figure 9. Typical droplet size distribution at the leading edge of the fully developed diesel injection spray

Previous work by the authors has extracted droplet size information from the microscope image analysis at the leading edge of the injection event [17]. A typical sample at 22mm downstream of the nozzle is presented in Figure 9, showing a distribution of small diesel droplets, having a Sauter mean diameter of 10.1microns.

Start of Injection

The focus of this work is to investigate the transient behavior of the diesel injection and the potential for CFD simulations to capture these off-design phenomena. This combination of analyses will offer a more detailed holistic understanding. In contrast to fully developed sprays, the early stages of injection does not contain the range of small droplets observed in Figures 8 and 9, but larger structures, liquid core and ligaments, from which droplets will be created within the breakup regimes. The shadowgraph images from a single hole of the injector nozzle shown in Figure 10 illustrate the early developing spray at an injection pressure of 400bar, being representative of light load and idle conditions. Detailed aspects of this spray development and structure are discussed in [14].
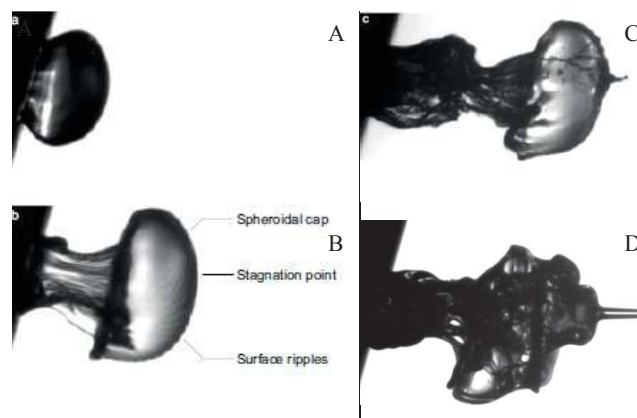

Figure 10. High-resolution microscopic image showing the structure of the fuel during the early stages of injection (Pinj = 400 bar, ICP = 1 bar) [14]

As injection commences the needle lifts off its seat and the nozzle pressure will increase leading to the fuel starting to flow within the nozzle holes. Initially, if the fuel in the channels which form the nozzle holes is in the liquid phase, it will slowly exit, spreading into apart-spherical shape, prior to being lifted from the surface of the injector and pushed through the gas by the momentum of the following liquid core. This sequence of events can be seen in Figures 10a and 10b where a liquid core, with a similar cross-section to the nozzle hole area, emerges fronted by an approximately hemi-spheroidal, or mushroom-shaped cap.. Figures 10c and d show the initial stages of instabilities in the liquid core as the flow and shear rates increase and primary breakup ensues.

The main features of the evolution of the fuel flow from the nozzle hole, described above, are captured qualitatively within the images from the CFD simulation shown in Figure 11. The images represent an iso-surface of the fuel in the early stages of the injection process. The needle lift is around 10 microns, as illustrated within the insets, and hence will still be throttling the flow. The development of the large spikes emanating from the head of the 'plug' of liquid in Figure 11 can be seen in the microscope images of Figure 10c and 10d (it should be borne in mind that the simulated and 'measured' injectors are not identical and so some detailed differences in the emergent flow structures are to be expected).
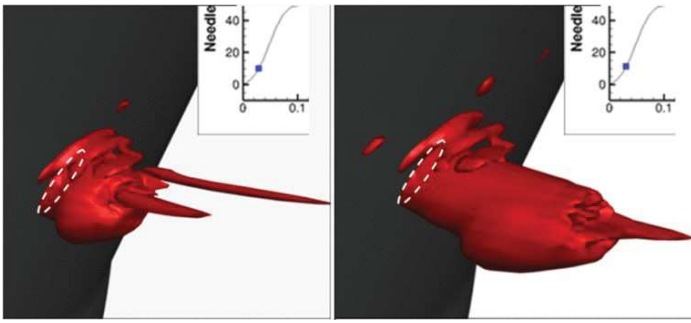
Figure 11. Iso-surface image from CFD simulation during early part of the injection process. 1600 bar into air at 60 bar and 353K – Isothermal conditions.

Since the CFD has isothermal boundary conditions the comparison with measured images taken under atmospheric conditions can be justified. This approach was employed since it simplified the overall simulation. For this initial study, simplification was sought to off-set the adverse influence on run time caused by the extremely fine mesh density, required to characterize the geometry and capture the flow features of interest, as discussed in the CFD section. Further simulations are planned which incorporate heat transfer and evaporation models. It is hoped these simulations will capture the evaporation of the fuel at the leading edge of the emergent liquid plug,as observed in Figure 12. In this image it can be seen that a cloud of gaseous phase fluid is emitted at the start of the injection event, through which the liquid fuel eventually penetrates due to its greater momentum. It is likely that the initial gaseous-phase cloud is vaporized fuel which has been resident within the sac volume of the fuel injector since the end of the previous injection event. The vortices formed within this residual vapour cloud as it is ejected from the nozzle hole can also be seen to follow a similar structure to that of the mushroom-shapedliquid head seen in the atmospheric case (Figure 10) and CFD simulations (Figure 11).
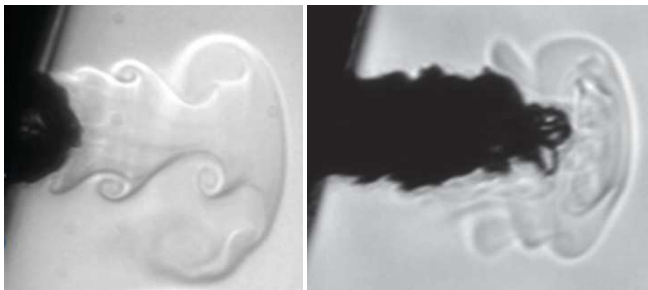

Figure 12. High-resolution microscopic image of diesel fuel injected at 400bar into air at 32bar ICT 700K [14].

When including evaporation models it is clearly important to include appropriate thermal boundaries for the operating conditions within CFD simulations and will form part of future work. A detailed map of the injector tip temperature was measured for a range of loads and speeds. Representative cycle-average temperature profiles are shown in Figure 13 to illustrate the extremes of thermal boundary conditions. This data was extracted from thermal mapping of the injector tip of a test bed engine with production calibration. The lowest temperature measured was 150°C, present at the low load/speed engine operating condition, with a 100°C temperature range observed up to the high load/speed condition. Even though the boiling point of the heavier fractions in diesel fuel distillation would exceed the upper limit of approximately 250°C, even at ambient

pressure, this does not preclude their evaporation since the measurement is a cycle average value and is 1mm below the metal surface.
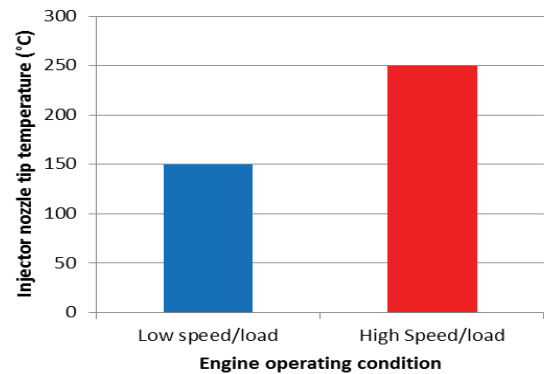

Figure 13. Measurements of nozzle temperature for a VCO-type diesel injector across the operating envelope within a modern diesel engine.

It is clear from the above that an important consideration for the simulation is the initial condition of the fluid within the nozzle holes. For this simulation the holes are completely filled with liquid fuel at the start of the calculation. It is assumed that in reality there will be a mix of fuel, gas and fuel vapour, which will evolve as the simulation progresses, and will be revisited in the next section. The initial condition within the nozzle holes will have implications for the spray development between close-coupled sequential injections within a multiple injection sequence, with a mix of effects such as those observed in Figures 10 and 12. It is expected the balance of liquid to vapour will be different for cold start and during the warm up events. The phase of the fluid within the nozzle holes of the injector after the end of an injection event is discussed later in the paper – this pre-conditions the fluid state at the beginning of the next injection event.

End of Injection

Once the driving current is removed from the injector the closing event commences. Figure 14 shows the spray dynamics as it collapses at the end of the injection process. Image A shows initial collapse of the developed spray structure as the needle starts to throttle the flow. The retraction of the spray liquid core towards the nozzle hole exit occurs in a disordered manor. The next image (B) shows the ensuing break-up of the liquid core into a swirling 'sheet' as the injector needle closes and the jet loses momentum. This sheet break-up process generates multiple connected ligaments of liquid fuel, which gradually degenerate beyond the end of the injection event (C and D) into large liquid droplets or long ligaments. These droplets have been shown to be in the order of 10 times larger than the finely atomised droplets on the edge of the full developed spray shown in Figure 8. The large, slow moving liquid structures have the potential to contact the injector surface in the near-nozzle region where they can contract due to surface tension effects and leave liquid globules in the near-nozzle region leading to wetting of the surface [13].

The jet collapse and eventual breakup of a swirling spray as outlined in Figure 14 A and B can be observed within the CFD simulations (Figure 15). As the needle closes and nears the reseating position the iso-surface image in Figure 15 A can be seen to show a twist which is evidence of the development of a swirling flow at the nozzle exit hole. Soon afterwards, the swirling structure breaks down into large

elements with tangential momentum but little forward impetus (Figure 15 B). The resultant long, slow moving ligaments present in Figure 15C have a relatively large fuel mass compared with the fine droplets of the fully developed fuel spray (see earlier). Some of these large droplets and ligament structures can be seen to have landed on the nozzle outer surface causing wetting. Similar large ligament structures have also been captured in the end of injection sequences from the near nozzle microscope measurements (Figure 15 D).

The swirling spray structure evident in both the simulation results and the measurements is a result of the throttling effect by the needle as it reaches its seating position, and the internal geometry of the diesel injector. The flow passing between the needle and nozzle internal wall must turn through close to 90° to pass along the nozzle holes, this process is accentuated within a VCO design.

At a needle lift of 5microns the needle is close to its seating position and the fluid stream lines shown in Figure 16 clearly show the pathway of fuel passing down through the injector. The downward tightly confined trajectory of the fuel flow between the injector body and the needle rapidly turns into each of the nozzle holes where there is evidence of swirl motion in all holes, at this stage of the closing event [24, 25, 26]. Some have a much tighter sequence of stream lines indicating a high swirl intensity, leading to the break-up phenomena at the hole exit described above. One further observation is that, even at this relatively late, slower flow condition, there are axial velocity magnitudes exceeding 100m/s. Equally there is evidence of low velocity fluid moving in a tangential direction from the nozzle hole exit.

The general characteristics of the fuel atomisation at the start and end of the injection event can be seen to be very different from those of the main part of the injection event, when the spray is essentially fully developed. Larger-scale structures are evident in both the simulation images and those of the flow in the real injector, shown in Figures 10-16, which can lead to reduced mixture preparation quality and, in some cases, fuel deposition on the surface of the injector.

A: (1.25ms ASOI)   B: (1.30ms ASOI)

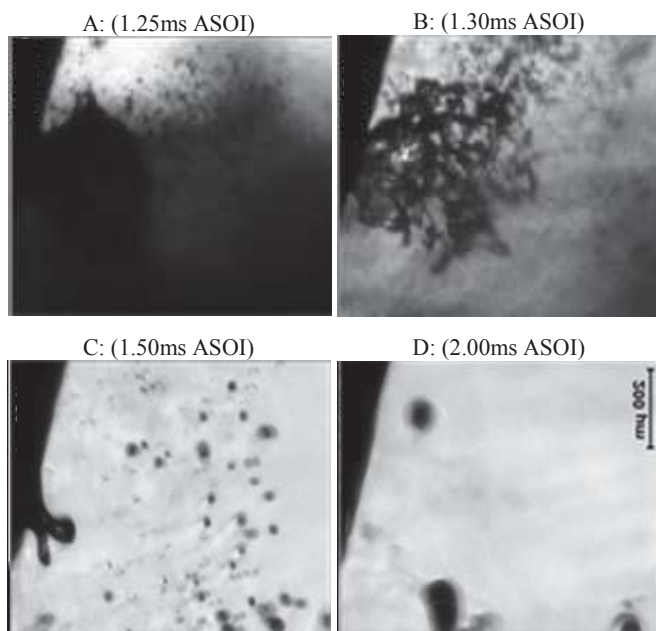C: (1.50ms ASOI)   D: (2.00ms ASOI)

Figure 14. Microscopic imaging around one nozzle hole capturing the transient phenomena during the injection closing event [13]
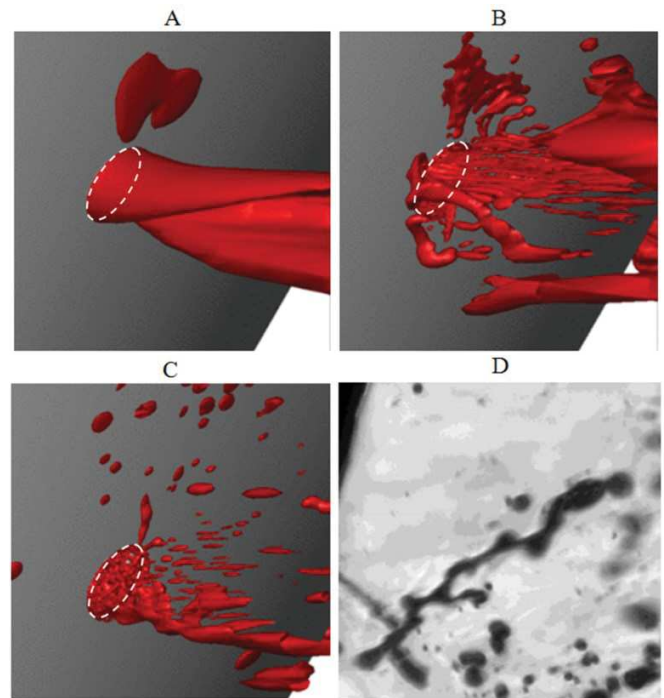
Figure 15. CFD simulation of the injection closing event, with large droplets and ligaments. Experimental measurement of a near nozzle ligament structure
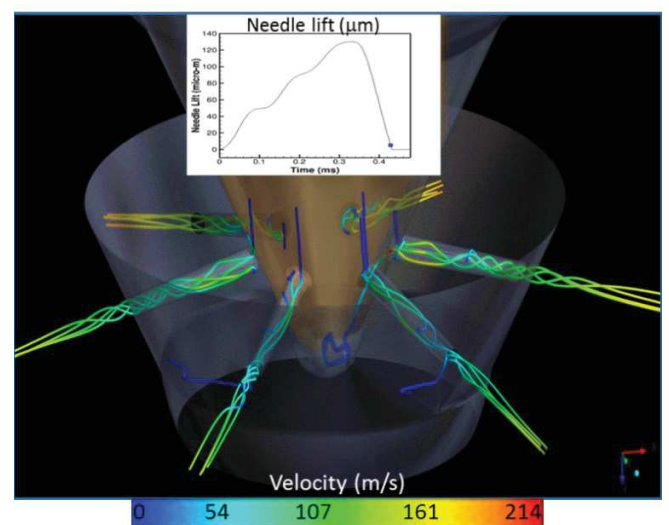

Figure 16. Stream-lines of internal nozzle flow showing rotating structure as needle closes.

After the End of Injection

As the needle descends within the injector and meets its seat the spray decays, culminating in a post-injection fluid discharge in contact with the near-nozzle region and causing surface wetting. Experimental data from real injectors can only shed light on the external features of the flow, while CFD simulations can capture the details within the injector itself which lead to those behaviours. A sequence of predicted mixture density images from the needle seating and post-injection timing for the injection event are shown in Figure 17 with associated comparable images from the high-speed microscopy with a 700μs injection driving pulse duration.
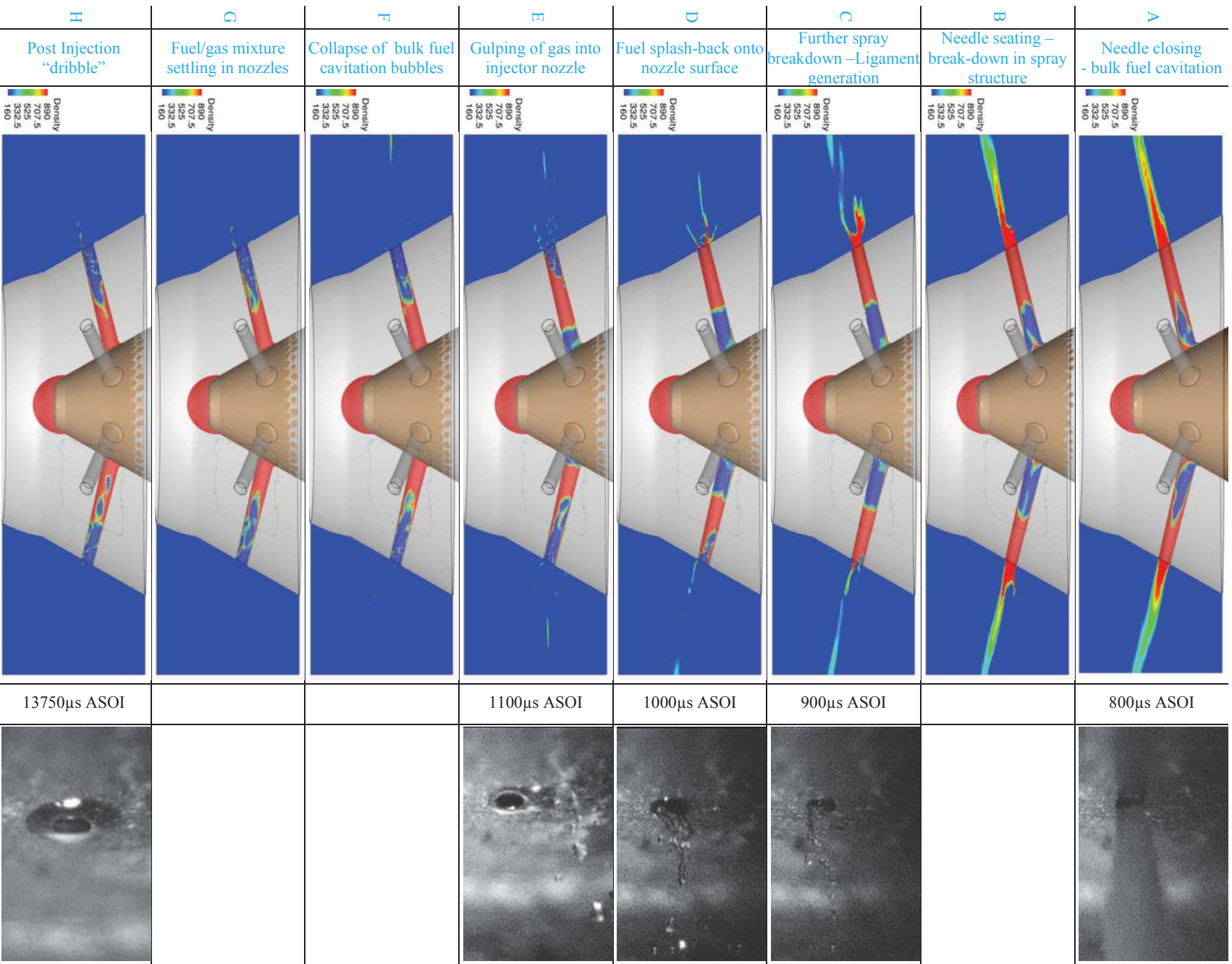
Figure 17: Details of CFD mixture density at the end of injection and associated microscope images, from needle closure to injection dribble.
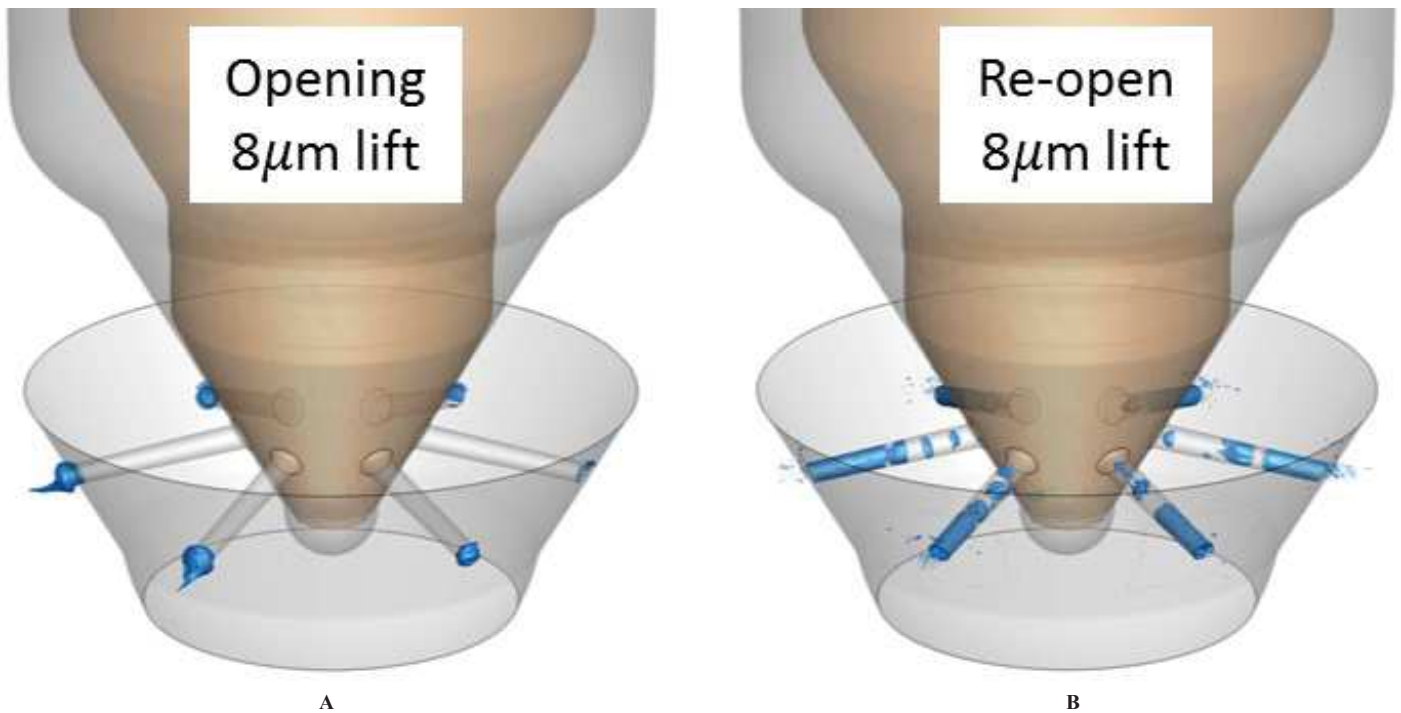
Figure 18: Comparison of nozzle conditions early in injection between an initial injection (eg. pilot) and subsequent injection (e.g. main). The blue colouring demarcates the interface between gas originally external to the injector and liquid fuel.

In Figure 17A the needle is at 10 micons lift, where the throttling of the fuel flow by the seating needle is creating a large region of low pressure at the each hole entry, with associated regions of fuel vapour or bulk fuel cavitation. The fuel spray will be starting to breakdown and soon develop the swirling patterns observed in Figure 16. The break down in fuel spray structure is clearly demonstrated in Figures 17B into 17C when the needle fully seats. At this point the external fluid momentum rapidly reduces with evidence of large ligament features downstream of the nozzle hole exit points, while the bulk cavitation occupies close to 50% of the nozzle volume. Transitioning from Figure 17C to 17D, the vapour region starts to retract and draw the final part of the fuel column back into the nozzle hole and as a consequence splashes fuel ligaments onto the outer surface of the injector body. These phenomena can also be observed within the microscope images shown on the right-hand side of Figure 17.

The vapour zone adjacent to the needle is close to collapse in Figure 17E. Its contraction has drawn the fuel column into the nozzle hole, together with some of the external gas. The existence of ingested gas has been identified in the literature [30, 34] and suggested as a possible source of discrepancy in validation of injection simulations [30]. In a fired engine this 'external gas' would consist of either air or hot post-combustion residual gas in the combustion chamber. In Figure 17F the vapour region previously adjacent to the needle has fully collapsed, with evidence of the liquid fuel and 'gulped' external gas mixing at the interface of the two phases. This mixing process continues into Figure 17G where some of the liquid fraction of the fuel starts to move once again towards the nozzle hole exit Finally in Figure 17H the internal fluid dynamics are settling and the remaining fuel can be seen to slowly 'dribble' out of the injector and wet the near nozzle surface. The surface wetting from post injection 'dribble' is in qualatitive agreement by the evidence from the experimental data.

The mix of liquid fuel, fuel vapour, and gas (air or combustion products) within the nozzle holes at the end of each injection will have a significant influence of the initial conditions within them for the next injection, and will have implications for the spray development between close-coupled sequential injections within a multiple injection sequence, as discussed above. Figure 18 compares the conditions within the nozzle holes at two stages of a simulation of a pair of close-coupled injection events. In Figure 18A the fluid in the nozzle holes is initialized in the model as being in the liquid phase. The blue colour indicates the iso-surface between the liquid fuel and the external gas (air in this case). Later in the simulation, at the start of the subsequent injection event (Figure 18B), the nozzle holes contain striations of liquid fuel and gas which has been retracted at various stages of the interval following the end of the previous (initial) injection event. A close investigation of the six nozzle holes around the injector it is possible identify the range and differentiation of liquid/vapour zones present within each hole, (2 are less clear due to the needle obscuration). These are a result of the air/vapour entrainment from the previous injection. Due to the stochastic nature of the end of injection events within each nozzle hole, it is difficult to estimate injector hole initial boundary conditions for injection simulations. It is for this reason the nozzle holes were initialised in the current simulation with pure liquid fuel at downstream pressure conditions.

The features of the post injection 'dribble' phenomena can be observed more clearly in Figure 19. The fuel can be seen to gulp out of the nozzle holes and run across the nozzle surface., This could be a result of the settling of the post-injection fluid dynamics. In other conditions the post-injection fuel emerges more slowly oozing out with the surface tension resulting in an adhesion of the liquid to the nozzle surface and retraction towards the orifice as seen in Figure 17.

Figure 19. Image sequence showing fuel discharge after needle closure

Surface Combustion

Figure 20 shows combustion of a collapsing fuel spray at the end of an injection event in a rapid compression machine (RCM) operating with elevated intake air to reach the conditions of auto-ignition. The conditions around the injector nozzle would represent the pressures and temperatures present during light load engine operation; however the intake derived swirl is not present in the RCM together with the mixing control and squish generated by a re-entrant piston bowl present in a modern diesel engine. These additional features will be captured within further investigations within a full optical engine.

In Figure 20A, while the injection is ending and the spray collapsing, it is possible to identify the main combustion zone downstream of the visible injected sprays in the lower right corner, within the mixed fuel vapour-air region. Moving to Figure 20B the injection has ended, as too has the main combustion event. The residual combusting mixture zones are carried in the bulk gas motion, and can be seen to traverse the injector nozzle. There appears to be combustion of what is thought to be liquid fuel which has spilled on to the injector outer surface following the events described above. The high temperature combined with oxygen dissolved in, or mixed with, the fuel, together with active chemical radials (such as NO_x) in the post-combustion gas, is thought to lead to oxidation of the fuel on the injector surface, forming polar proto-deposit initiators [16]

Following the end of injection, the microscopic measurements and simulation showed fuel dribble (Figure 17), which can eject small amounts of fuel from each nozzle into this surface combustion phenomena. In Figure 20C&D combustion ligaments can be identified emanating 2 of the lower left nozzle holes. These flare-type structures can be seen to stretch out with the local flow (right to left and down across the image) and combine into a diffusion cloud. This ultimately detaches from the flare structures and could be carried to late in an engine expansion stroke.

All of these combustion events will be diffusion-driven and will therefore result in rich, slower overall combustion, leading to the formation of particulates. This in combination with the proximity to the nozzle surface and holes can lead to deposit initiators and building blocks for further deposit accumulation.
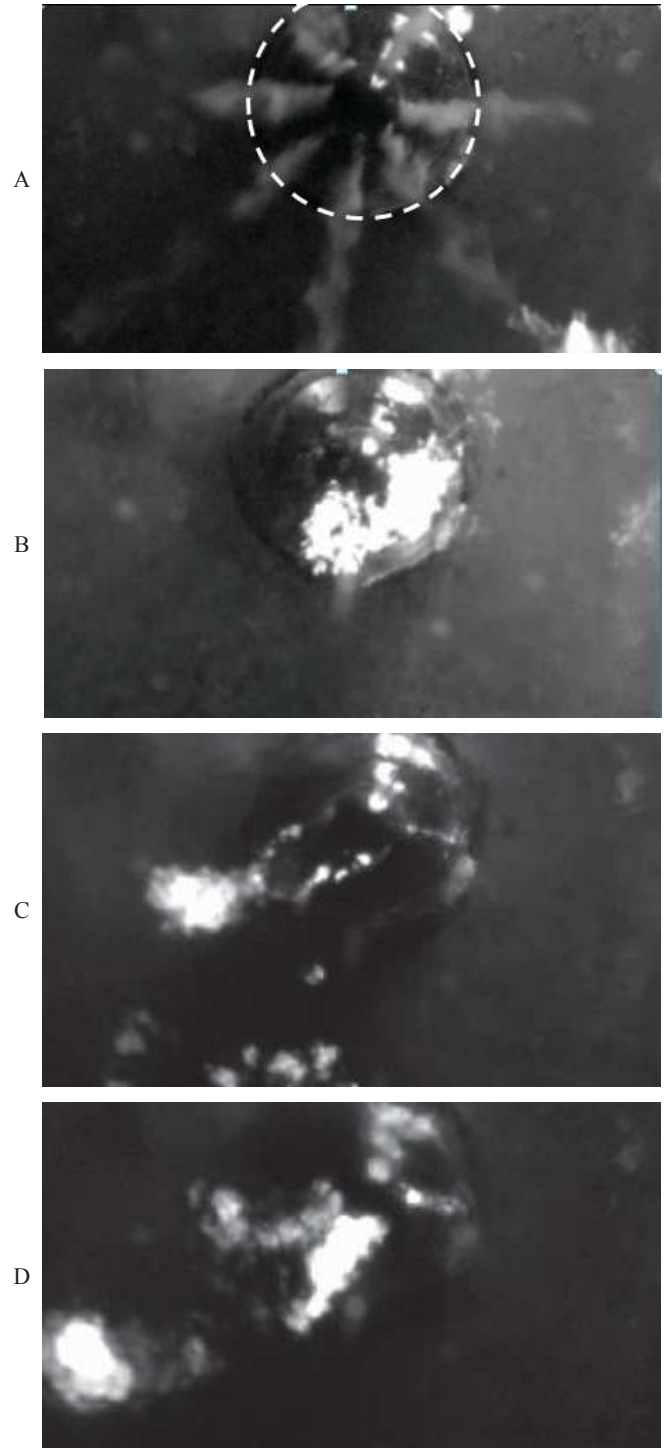

Figure 20. Image sequences showing combustion contacting the near nozzle region, with associated surface fuel combustion.

Conclusions

The combination of high-speed microscopy and use of CFD modelling has led to a detailed visualization and understanding of the fluid dynamics of fuel introduced in the early and late stages of diesel injection events. The following key insights have been identified in a VCO-type injector:

- The liquid fuel issuing from the injector at the start and end of the injection process is in the form of much larger structures than the finely atomized droplets produced in the main part of the event.

- High-speed microscopy can reveal detailed flow features at the start and end of the injection process which are of particular interest regarding their potential role in the formation of external injector deposits. These features can be reproduced by a CFD model with sufficient mesh refinement to characterize the injector geometry and dynamics, and capture robustly the fundamental fluid dynamic processes.

- Microscopic imaging and simulation show the development of a plug flow in the initial stages of injection, initially with a broad head which may be later penetrated by finer jets ('spikes') of high-momentum fuel. The subsequent transition into the primary breakup regime is rapid, with the large liquid structures transitioning to a finely atomised spray which facilitates vaporisation of the fuel.

- During closuring of the injector the spray collapses, with evidence of swirling breakup structures, shown clearly in the images from the CFD model. During this degeneration of the spray jet unstable ligaments of fuel break into large slow-moving droplets. This is thought to lead to sub-optimal combustion in the developing flame fronts established by the earlier, more fully-developed spray.

- The simulation results and microscopy images show injector surface wetting as a result of large slow-moving droplets and post-injection discharge of liquid fuel. These details suggest that surface wetting from the collapse of the spray jets and the post-injection discharge of fuel play a part in the mechanism of the initial formation, and subsequent accumulation of deposits on the exterior surface of the injector.

- The detailed images from the CFD model showing the mixture of fluid phases within the nozzle holes indicates that fluid state at the start of an injection event is pre-conditioned by the phenomena occurring at the end of the previous event and in the intervening time. This highlights the necessity to simulate multiple injection events to obtain downstream start of injection conditions that may exist within a real injector nozzle.

- A significant amount of cylinder gas can reside within the nozzle hole, which the new fuel injected in to the cylinder has to displace before if emerges from the hole exit. This will have significant impact in modern engines employing multiple injection strategies within one cycle.

Abbreviations

ASOI	After start of injection
BTDC	before top-dead-centre
CCD	Charge-coupled device
CFD	Computational fluid dynamics
DI	Direct injection
DRS	Digital rate shaping
EU	European Union
ICP	In-cylinder pressure
NCS	Needle closing sensor
Pinj	Injection pressure (main fuel rail)
RANS	Reynolds-averaged Navier-Stokes
RCM	Rapid compression machine
VCO	Valve-covered orifice
VOF	Volume of fluid

References

1. European Vehicle Market Statistics: Pocketbook 2015/16. ICCT. http://eupocketbook.theicct.org November 2015.

2. Zeh D, Hammer J, Uhr C, Ruckle M, Rettich A, Grota B, Stocklein W, Gerhardt J, Naber, D & Raff M, 'Bosch diesel injection technology – response for every vehicle class'. 23rd Aachen Colloquium: Automobile and Engine Technology, Aachen, 7th-8th October 2014.

3. Judge R, Beduneau J-L, Boncompte X, Cardon C, Dale M, Ralph M & Schiffgens H-J, 'The next generation of Delphi common rail systems for light and medium duty commercial vehicles'. 23rd Aachen Colloquium: Automobile and Engine Technology, Aachen, 7th-8th October 2014.

4. Schoppe D, Atzler F, Kastner O & Kapphan F, 'High performance diesel direct driven piezo common rail injection system'. 23rd Aachen Colloquium: Automobile and Engine Technology, Aachen, 7th-8th October 2014.

5. Piock W, Hoffmann G, Ramsay G, Millen R, Schilling S, Dalo D & Spakowski J, 'Delphi's fuel injection systems for efficient and clean gasoline engines with direct injection'. 36th International Vienna Motor Symposium, Vienna, 7th-8th May, 2015.

6. Eichler, F., Demmelbauer-Ebner, W., Theobald, J., Stiebels, B., Hoffmeyer, H., and Kreft, M., 'The new EA211 TSI evo from Volkswagen', 37th International Vienna Motor Symposium, Vienna, 28th-29th April 2016.

7. Eltel, F., Schafer, J., Konlgstein, A., Heeger, C., 'Fuel Pressure Increase up to 50MPa for Gasoline Direct-Injection Engines' – MTZ worldwide 07-08|2018: 50-55, 2018.

8. Maier R, Warga J, Pauer T, Gerhardt J & Kruger M, 'The next generation BOSCH common rail injectors with digital rate shaping – a key factor for meeting future requirements'. 33rd International Vienna Motor Symposium, Vienna, 26th-27th April, 2012.

9. Birgel A, Ladommatos N, Aleiferis P, Zulch S, Milovanovic N, Lafon V, Orlovic A, Lacey P & Richards P, 'Deposit formation in the holes of diesel injector nozzles: A critical review'. SAE paper no. 2008-01-2383, SAE International, Warrendale, PA., 2008.

10. Winterbone D, Clough E, Rao K, Richards P & Williams D, 'The effect of DI nozzle fouling on fuel spray characteristics'. SAE paper no. 922232, SAE International, Warrendale, PA., 1992.

11. Kalghatgi G, 'Fuel / Engine Interactions', SAE International, 2014. ISBN 978-0-7680-6458-2.

12. Smith A & Williams R, 'Linking the physical manifestation and performance effects of injector nozzle deposits in modern diesel engines'. SAE paper no. 2015-10-0892, SAE International, Warrendale, PA., 2015.

13. Crua C, De Sercey G, Gold M & Heikal M, 'Image-based analysis of evaporating diesel sprays in the near-nozzle region'. ILASS – Europe 2013, 25th European Conference on Liquid Atomization and Spray Systems, Chania, Greece, 1-4 September, 2013.

14. Crua C, Heikal M & Gold M, 'Microscopic imaging of the initial stage of diesel spray formation'. Fuel 157: 140-150, 2015.

15. Crua C, 'Combustion Processes in a Diesel Engine', in School of Engineering. 2002, University of Brighton: Brighton.

16. Slavchov R, Mosbach S, Kraft M, Pearson R & Filip S, 'An adsorption-precipitation model for the formation of injector external deposits in an internal combstion engine'. J. App. Energy, 228, 1423-1438, 2018.

17. Crua, C., De Sercey, G., Heikal, M. & Gold, M., 'Dropsizing of near nozzle diesel and RME sprays by microscopic imaging', ICLASS 2012, 12th Triennial International Conference on Liquid Atomisation & spray systems, Heidelberg, 2–6 Sept 2012

18. Koukouvinis P, Bruecker C & Gavaises M, 'Unveiling the physical mechanism behind pistol shrimp cavitation' Nature Scientific Reports, 7, Article number: 13994 (2017), doi:10.1038/s41598-017-14312-0

19. Murali-Girija M, Koukouvinis P & Gavaises M, 'Numerical simulation of cavitation and atomization using a fully compressible three-phase model', Physical Review Fluids, 3, 064304, DOI: 10.1103/PhysRevFluids.3.064304

20. Mittal, R. & Iaccarino, G. 'Immersed boundary methods'. Annual Review of Fluid Mechanics 37, 239-261, doi:10.1146/annurev.fluid.37.061903.175743 (2005).

21. Reboud J, Stutz B & Coutier-Delgosha O, 'Two phase flow structure of cavitation: experiment and modeling of unsteady effects', 3rd International Symposium on Cavitation, CAV1998 26 (1998).

22. Wilcox D, 'Turbulence modeling for CFD,' D C W Industries (2006), ISBN 9781928729099.

23. Koukouvinis P, Naseri H & Gavaises M, 'Performance of Turbulence and Cavitation Models in Prediction of Incipient and Developed Cavitation', International Journal of Engine Research, 2016, doi: 10.1177/1468087416658604.

24. Andriotis, M. Gavaises, and C. Arcoumanis, 'Vortex flow and cavitation in diesel injector nozzles', J. Fluid Mech., vol. 610, pp. 195–215, Aug. 2008

25. Battistoni M, Xue Q, Som S & Pomraning E, 'Effect of Off-Axis Needle Motion on Internal Nozzle and Near Exit Flow in a Multi-Hole Diesel Injector', SAE Int. J. Fuels Lubr. 7(1):2014, doi:10.4271/2014-01-1426

26. Theodorakakos A, Gavaises M, Pearson R & Gold M, 'Influence of fuel composition on cavitation inception and further development in diesel fuel injectors', IMechE 2015.

27. Battistoni M, Xue Q & Som S, 'LES of Spray Transients: Start and End of Injection Phenomena', Oil & Gas Science Technology, Rev. IFP Energies Nouvelles (2016) 71, 4, doi:10.2516/ogst/2015024

28. Battistoni M, Poggiani C & Som S, (2016), "Prediction of the Nozzle Flow and Jet Characteristics at Start and End of Injection: Transient Behaviors," SAE Int. J. Engines 9(1):2016,doi:10.4271/2015-01-1850

29. Fischer A & Thelliez M, "Methodology and Tools to Predict GDI Injector Tip Wetting as Predecessor of Tip Sooting,"SAE Technical Paper 2018-01-0286, 2018, doi:10.4271/2018-01-0286

30. Ghiji M, Goldsworthy L, Brandner P, Garaniya V & Hield P, 'Numerical and experimental investigation of early stage diesel sprays', Fuel 175 (2016) 274–286

7/20/2015

31. Ghiji M, Goldsworthy L, Brandner P, Garaniya V & Hield P, Analysis of diesel spray dynamics using a compressible Eulerian/VOF/LES model and microscopic shadowgraphy', Fuel 188 (2017) 352–366

32. Manin J, Pickett L & Yasutomi K, 'Transient cavitation in transparent diesel injectors', ICLASS 2018, 14th Triennial International Conference on Liquid Atomization and Spray Systems, Chicago, IL, July 22-26, 2018.

33. Papadopoulos N & Aleiferis P, 'Numerical Modelling of the In-Nozzle Flow of a Diesel Injector with Moving Needle during and after the End of a Full Injection Event', SAE Int. J. Engines 8(5):2285-2302, 2015, https://doi.org/10.4271/2015-24-2472.

34. Swantek A, Duke D, Tilocco F, Sovis N, Powell C & Kastengren A, 'End of Injection, Mass Expulsion Behaviors in Single Hole Diesel Fuel Injectors', ILASS Americas, 2014.

35. Moon S, Gaob Y, Park S, Wang J, Kurimoto N, Nishijima Y, 'Effect of the number and position of nozzle holes on in- and near-nozzle dynamic characteristics of diesel injection', Fuel 150 (2015) 112–122

36. Pos R, Avulapati M, Wardle R, Cracknell R, Megaritis T, Ganippa L, 'Combustion of ligaments and droplets expelled after the end of injection in a multi-hole diesel injector', Fuel 197 (2017) 459–466

37. Ubbink O, "Numerical Prediction of Two Fluid Systems with Sharp Interfaces", Imperial College London, PhD thesis, 1997.

Contact Information

Dr Martin Gold

BP Formulated Products Technology

Research & Innovation , BP Formulated Products Technology, Technology Centre, Whitchurch Hill, Pangbourne, Berkshire, RG8 7QR United Kingdom

Phone: +44(0) 2034013681

Email: martin.gold@uk.bp.com